



Article

Integrated Metabolome and Transcriptome Analyses Reveal That the Flavonoid Metabolic Pathway Is Associated with Pigment Differential Accumulation in Two Colors of Petaloid Staminodes in *Canna glauca*

Tong Zhao ¹, Zehong Wei ², Huanfang Liu ³ and Limei Dong ^{1,*}¹ Guangdong Eco-engineering Polytechnic, Guangzhou 510520, China² Guangdong Mechanical & Electrical Polytechnic, Guangzhou 510520, China³ Key Laboratory of Plant Resources Conservation and Sustainable Utilization, South China Botanical Garden, Chinese Academy of Sciences, Guangzhou 510650, China

* Correspondence: dlm0728@163.com

Abstract: *Canna glauca*, an ornamental plant widely cultivated in aquatic habitats, is notable for its long florescence and showy flowers. The flower of this species is distinguished by its petaloid staminodes, which comprise the majority of the overall floral display. Flavonoids have been reported to be the predominant pigment groups that determine most flower colors. However, the influence of flavonoid metabolic pathways on the flower color of *C. glauca* remains to be investigated. In this study, comprehensive floral transcriptomes and metabolite profiles of the wild type (yellow flower) and ‘Erebus’ cultivar (pink flower) of *C. glauca* were analyzed. We identified 432 flavonoid metabolites, including 20 anthocyanins. ‘Erebus’ accumulated higher levels of 18 anthocyanins than the wild type, including 10 cyanidins, 4 pelargonidins, and 4 peonidins. The wild type accumulated higher levels of two malvidins. Through the joint analysis of transcriptomics and metabolomics, we observed a notable association between the expression of three DEGs and eleven anthocyanin levels. Furthermore, we analyzed the expression patterns of key genes that determine flavonoid biosynthesis, such as *CHS*, *CHI*, *F3'H*, and *DFR*. These findings provide enlightenment on the anthocyanin accumulation of *Canna glauca*, serving as a basis for exploring biochemical and molecular mechanisms underlying flower coloration.

Keywords: *Canna glauca*; anthocyanins; flavonoids; transcriptomic; metabolomic; petaloid staminodes



Citation: Zhao, T.; Wei, Z.; Liu, H.; Dong, L. Integrated Metabolome and Transcriptome Analyses Reveal That the Flavonoid Metabolic Pathway Is Associated with Pigment Differential Accumulation in Two Colors of Petaloid Staminodes in *Canna glauca*. *Horticulturae* **2024**, *10*, 372. <https://doi.org/10.3390/horticulturae10040372>

Academic Editor: Nakao Kubo

Received: 22 February 2024

Revised: 31 March 2024

Accepted: 4 April 2024

Published: 7 April 2024



Copyright: © 2024 by the authors. Licensee MDPI, Basel, Switzerland. This article is an open access article distributed under the terms and conditions of the Creative Commons Attribution (CC BY) license (<https://creativecommons.org/licenses/by/4.0/>).

1. Introduction

The order Zingiberales comprises plants predominantly distributed in subtropical and tropical regions. It can be further classified into two subgroups: the “ginger group” and the “banana group”. The former includes Marantaceae, Cannaceae, Costaceae, and Zingiberaceae families, while the latter consists of Musaceae, Strelitziaceae, Heliconiaceae, and Lowiaceae families [1–3]. One notable characteristic shared by families within the ginger group is the presence of petaloid staminodes. In the mature flowers of these plants, these petaloid staminodes replace most of the stamens [4,5]. *Canna glauca*, a perennial herb in the Cannaceae family, is renowned for its long florescence and showy flowers, particularly in aquatic environments. The unconventional petaloidy among the androecial members, comprising a fertile stamen and multiple staminodes, contributes to the floral manifestation in *C. glauca*. *C. glauca* is composed of four floral whorls (Figure 1a); the outer perianth consists of three sepals, while the inner perianth is made up of three petals. The androecial whorl contains one fertile stamen and four staminodes, which can be further divided into two trimerous whorls. The lateral staminode in the outer androecial whorl develops into two laminar (petaloid) floral organs, while the other staminode ceases development shortly after initiation [4,5]. The inner whorl comprises a curved staminode,

namely the ‘labellum’, a petaloid staminode, and a fertile stamen bearing a one-theca fertile anther and a sterile petaloid appendage. The innermost whorl of the flower is a tricarpeillary pistil. The morphological anatomy of the native species with yellow flowers (Figure 1b) and the cultivar ‘Erebus’ with pink flowers (Figure 1c) are respectively shown in Figure 1d,e and Figure 1f,g. These staminodes with vibrant colors usually constitute the visually striking part of the overall floral display, serving as optic signals to attract pollinators. Currently, the native species with yellow flowers and the cultivar ‘Erebus’ with pink flowers are extensively cultivated in aquatic habitats, and the formation mechanism of color difference between these two is still poorly understood.

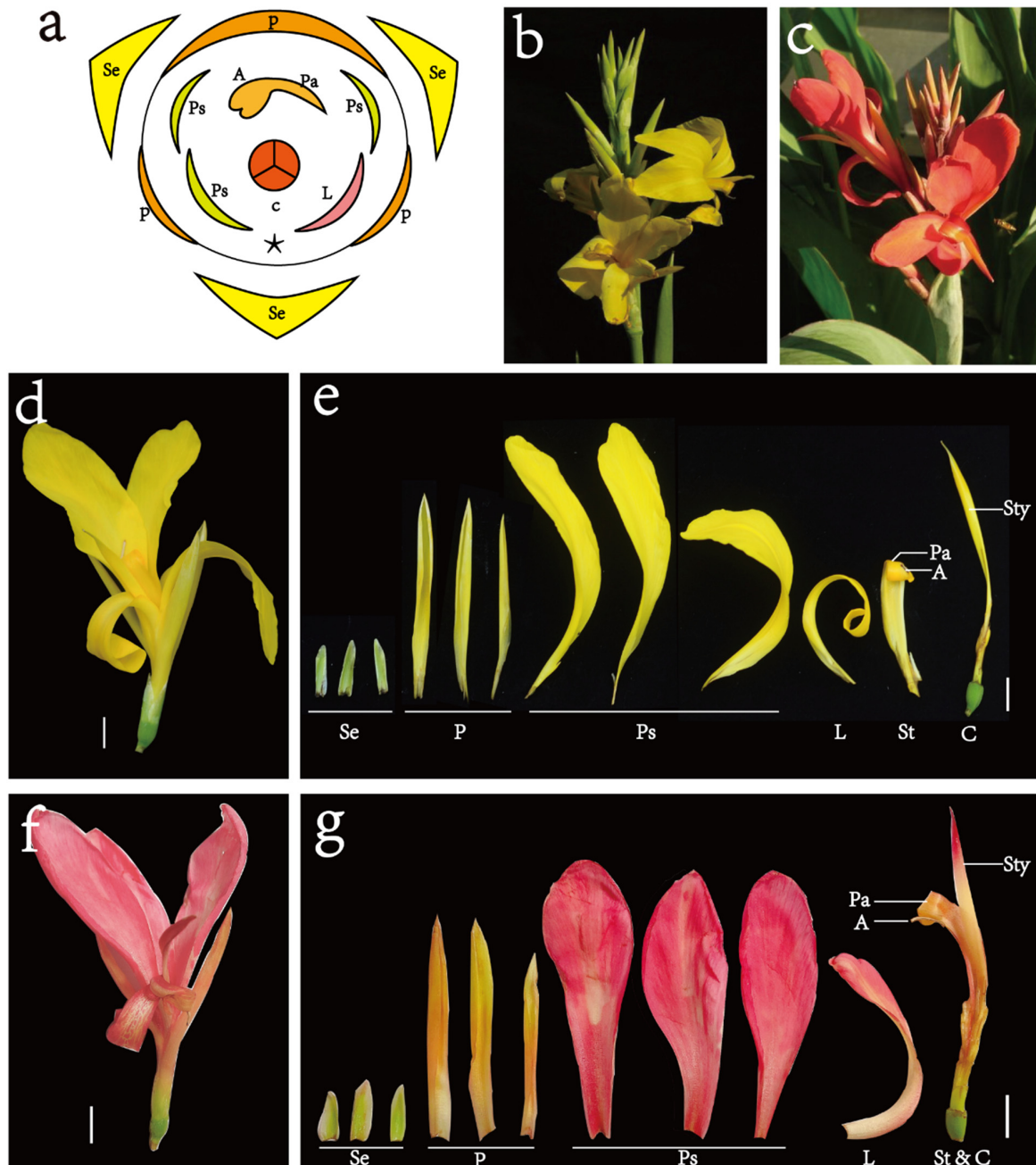


Figure 1. Floral morphology of *C. glauca*. (a) Floral diagram of *C. glauca*; (b) inflorescence of the *C. glauca* wild type; (c) inflorescence of the *C. glauca* ‘Erebus’ cultivar; (d,e) morphological anatomy of *C. glauca* wild-type flowers; (f,g) morphological anatomy of *C. glauca* ‘Erebus’ flowers. p: petal, Se: sepal, Ps: petaloid staminode, L: labellum, sty: style, A: anther, st: stamen, Pa: petaloid appendage, C: carpel. The asterisk indicates the degenerated abaxial staminode.

Floral coloration in most flowering plants is primarily determined by the accumulation of natural pigments, including anthocyanins, flavonoids, and their derivatives. Among these, flavonoids play a vital role, exhibiting a diverse array of colors such as orange, blue (through anthocyanins), and yellow (through chalcones, aurones, and flavonols), making them the predominant pigment groups responsible for flower color [6]. The specific combination and concentration of anthocyanins in the petals contribute to the wide variety of colors we see in nature. These pigments not only attract pollinators but also serve as a protective mechanism against UV radiation and other environmental stresses [7]. Among the six primary anthocyanins in plants—pelargonin, delphinidin, malvidin, peonidin, petunidin, and cyanidin—peonidin is generated through cyanidin methylation, whereas petunidin and malvidin are formed through different forms of delphinium methylation [6,8]. Peonidin and cyanidin display hues spanning from purple to red, whereas pelargonin manifests as a brick-red hue. Delphinidin, malvidin, and petunidin display hues falling between blue and purple. These compounds modify plant pigmentation and induce shifts from pink to blue [9,10].

The core flavonoid biosynthetic pathway is well understood [11–13]. It involves a chain of enzymatic reactions that transform phenylalanine into various flavonoid compounds, including anthocyanins, flavonols, and flavones. This pathway has been extensively investigated and characterized across diverse plant species [14–17]. The key enzymes in this pathway are phenylalanine ammonia-lyase (*PAL*), chalcone synthase (*CHS*), chalcone isomerase (*CHI*), flavanone 3-hydroxylase (*F3H*), flavonoid 3'-hydroxylase (*F3'H*), anthocyanidin synthase (*ANS*), and dihydroflavonol 4-reductase (*DFR*) [18,19]. These enzymes catalyze specific reactions and give rise to specific pigmentation patterns like stripes or spots, ultimately determining the flower color and pattern in plants. While there have been numerous reports explaining flower color at the molecular level via the flavonoid biosynthetic pathway [20–22], it is necessary to consider the variation among different plant species as there are no universal rules. Each plant species may have different metabolic processes and genes that regulate pigments; therefore, a personalized analysis is necessary for understanding the flower color of *C. glauca*. UPLC/ESI-Q TRAP-MS/MS, as a highly effective technique for metabolite identification and analysis, has been widely applied in different plants like lily, tree peony, tomato, and strawberry [23–26]. To analyze the differences in pigmentation patterns between the wild type and the 'Erebus' cultivar, we integrated flavonoid metabolomics and transcriptomics to elucidate the underlying metabolic pathways and potentially identify key genes or enzymes responsible for the observed variations in *C. glauca* flower coloration. This study identified the major anthocyanin categories in the petaloid staminodes of the wild type and 'Erebus' cultivar of *C. glauca*, established the flavonoid metabolomic profile and transcriptomic library of *C. glauca*, and identified key candidate genes and transcription factors involved in the differential accumulation of anthocyanins, which enhance our comprehension of the molecular mechanisms underlying flower color variations, offering guidance for further research into plant genetics and the horticultural breeding of *Canna*.

2. Materials and Methods

2.1. Plants

C. glauca was grown at Guangdong Eco-engineering Polytechnic, Guangzhou, China. Fresh petaloid staminodes of the wild type (CgpsY) and 'Erebus' cultivar of *C. glauca* were gathered in 2023 from May to June. Three biological replicates of petaloid staminodes of the wild type and 'Erebus' cultivar were collected, flash-frozen in liquid nitrogen for over 30 min, and preserved at -80°C .

2.2. Flavonoid Metabolite Extraction and Analysis

Petaloid staminode tissues were crumbled using a lyophilizer (Scientz-100F, Scientz, Ningbo, China) and pulverized for 1.5 min at 30 Hz into powder form. Subsequently, 50 mg of the powder was resuspended in 1.2 mL of 70% methanol aqueous solution, mixed

vigorously for 30 s every 30 min, repeating the process six times, and then centrifuged at 12,000 rpm for 3 min. The resulting supernatants were then filtrated via a 0.22 μm microporous membrane (SCAA-104; ANPEL, Shanghai, China).

For UPLC-ESI-MS/MS analyses (SCIEX, ExionLCTM AD, Sciex, Ningbo, China), 2 μL of the filtrated sample was injected onto an Agilent SB-C18 column (1.8 μm , 2.1 mm \times 100 mm) and segregated at 40 $^{\circ}\text{C}$ in a mobile phase composed of pure water with 0.1% formic acid and acetonitrile with 0.1% formic acid at 0.35 mL/min under a gradient program configured at 95:5 at 0 min, 5:95 at 9 min, and 95:5 at 11.1 min. The resulting effluent was alternatively subjected to ESI-triple quadrupole linear ion trap mass with a source temperature at 500 $^{\circ}\text{C}$, an ion spray voltage (IS) at 5500 V (positive ion mode)/−4500 V (negative ion mode), an ion source gas I at 50 psi, gas II at 60 psi, and curtain gas at 25 psi, and collision-activated dissociation at a high level. Triple quadrupole (QQQ) scans were obtained through multiple reaction monitoring experiments with medium collision nitrogen gas. Declustering potential and collision energy were optimized for single multiple reaction ion monitoring mode (MRM) transitions.

2.3. Differential Metabolite Identification

Differential metabolites between the two groups were determined based on the criteria of variable importance in projection (VIP) ≥ 1 and $|\text{Log}_2\text{FoldChange}| \geq 1.0$. VIP values were derived from OPLS-DA comprising score plots and permutation plots generated by the R package MetaboAnalystR. Prior to OPLS-DA, data were log₂-transformed and mean-centered. A total of 200 permutations were used in the permutation test to prevent overfitting. The heatmap depicting differentially accumulated flavonoid metabolites was generated using TBtools v2.010 [27].

2.4. Transcriptome Sequencing

RNA samples were obtained from CgpsY and CgpsP using the RNA plant plus kit (TIANGEN, Beijing, China) and purified with oligo(dT) magnetic beads. After fragmentation via divalent cations at high temperatures, mRNA was converted to double-stranded cDNA with random hexamer primers, DNA polymerase I, and Rnase H. The obtained cDNA was purified with the QiaQuick PCR extraction kit (Qiagen, Venlo, The Netherlands), end-repaired, and added to poly(A) tails [28]. The libraries were prepared via Illumina sequencing adapter ligation, agarose gel electrophoresis, and PCR amplification [28] and sequenced on the Illumina platform to generate 150 bp paired-end raw reads. After eliminating adapters, unknown nucleotides, and poor-quality sequences, clean reads were obtained and assembled using Trinity v2.4.0 [29].

2.5. Gene Annotation and Differentially Expressed Gene Identification

BLASTx against NCBI non-redundant protein sequences (NR), Swiss-Prot, Protein family (Pfam), euKaryotic Ortholog Groups (KOG), and Kyoto Encyclopedia of Genes and Genomes (KEGG) was used for gene functional annotation. The Blast2GO 2.3.5 program was used for Gene Ontology (GO) annotations [30]. TransDecoder was used for coding DNA sequence (CDS) prediction to identify candidate coding regions with transcript sequences. Transcription factor analysis was conducted using iTAK software (<https://omictools.com/itak-tool>, accessed on 25 August 2023). Relative gene expression was evaluated using the fragments per kilobase of transcript per million mapped reads (FPKM) approach [31]. edgeR package was utilized to identify differentially expressed genes (DEGs), with selection criteria of at least 2-fold change and a false discovery rate < 0.05 [32].

2.6. Real-Time Quantitative PCR

The levels of 9 selected unigenes (Cluster-17340.2, Cluster-16437.0, Cluster-13713.0, Cluster-15881.0, Cluster-16437.1, Cluster-34059.0, Cluster-23068.0, Cluster-19592.3, and Cluster-20066.0) were confirmed via qRT-PCR using specific primers designed with the Integrated DNA Technologies PrimerQuest tool (Supplementary Table S1). qRT-PCR was

performed with three parallel replicates in 20 μL solution containing 10 μL of Hieff[®] qPCR SYBR Green Master Mix (Yeasen Biotech, Shanghai, China), 0.5 μL of 10 μM of each primer, and 4 μL of cDNA template on a LongGene Q2000B Real-time PCR Detection system (LongGene Instruments, Hangzhou, China) under 40 cycles of 10 s at 95 °C and 30 s at 60 °C after 3 min at 95 °C. The level of each gene was normalized to the β -actin gene (Cluster-20989.10) using the Ct method [33]. Statistical significance was analyzed through an independent-samples *t*-test in SPSS Statistics 17.0.

2.7. Correlation of DEGs with Metabolites

The correlation analyses were performed with the quantitative values of metabolites and genes in total samples as the basis. The cor function in R was applied to compute the Pearson correlation coefficient of DEGs with metabolites and to select the correlation result with the criterion of an absolute value ≥ 0.8 and a *p*-value ≤ 0.05 .

3. Results

3.1. Flavonoid Metabolic Differences between the Wild Type and the 'Erebus' Cultivar of *C. glauca*

The flavonoid metabolite differences between the petaloid staminode of the wild type (CgpsY) and 'Erebus' cultivar (CgpsP) were investigated in this study with three biological replicates to reduce the impact of individual variations. A total of 432 flavonoid metabolites were uncovered (Supplementary Table S2), including 20 anthocyanins, 11 biflavones, 13 chalcones, 20 flavanols, 35 flavanones, 10 flavanonols, 142 flavones, 154 flavonols, 8 proanthocyanidins, 18 tannin, and 1 other flavonoid. Using the identification criteria of $\text{VIP} \geq 1$ and $|\text{Log}_2\text{FC}| \geq 1.0$, 238 flavonoid metabolites showed statistically significant differences in CgpsP vs. CgpsY (see Supplementary Table S3), of which 187 demonstrated significantly higher accumulation and 51 displayed significantly lower accumulation (Supplementary Figure S1), indicating that flavonoid compounds in petaloid staminodes of the 'Erebus' cultivar are more abundant than those of the wild type. A total of 20 anthocyanins, including cyanidin, peonidin, pelargonidin, malvidin, and their derivatives, demonstrated a significant difference in CgpsP vs. CgpsY. Eighteen anthocyanins were up-accumulated in CgpsP, mainly cyanidin (10 compounds), pelargonidin (4 compounds), and peonidin (4 compounds). Malvidin-3-O-galactoside and malvidin-3-O-glucoside were the only two anthocyanins to exhibit significant downregulation in CgpsP. The differentially accumulated flavonoids (DAFs) with $|\text{Log}_2\text{FC}| > 4$ are demonstrated in Figure 2. Biflavones (7 out of 8 compounds), flavones (16 out of 52 compounds), and flavonols (21 out of 97 compounds) detected in DAFs displayed significant down-accumulation in CgpsP. However, significant up-accumulation of chalcones (all 10 compounds), flavanols (all 10 compounds), flavanones (19 out of 21 compounds), flavanonols (5 out of 6 compounds), flavones (36 out of 52 compounds), and flavonols (76 out of 97 compounds) in CgpsP vs. CgpsY was observed.

According to the fold change value, the top three up-accumulated metabolites in CgpsP vs. CgpsY are cyanidin-3-O-arabinoside, cyanidin-3-O-xyloside, and peonidin-3-O-rutinoside (Figure 3). These metabolites are significantly increased in CgpsP, suggesting that they may contribute to the accumulation of pink pigments. 8-prenyl-7,4'-dihydroxy-5-methoxydihydroflavonol, gossypetin-8-O-glucoside, and Tricin-4'-O-glucoside showed a significant reduction in CgpsP (Figure 3), indicating their possible involvement in the accumulation of yellow pigments. These DAFs might be the major metabolites that affect the different coloration patterns of the wild type and 'Erebus' cultivar of *C. glauca*.

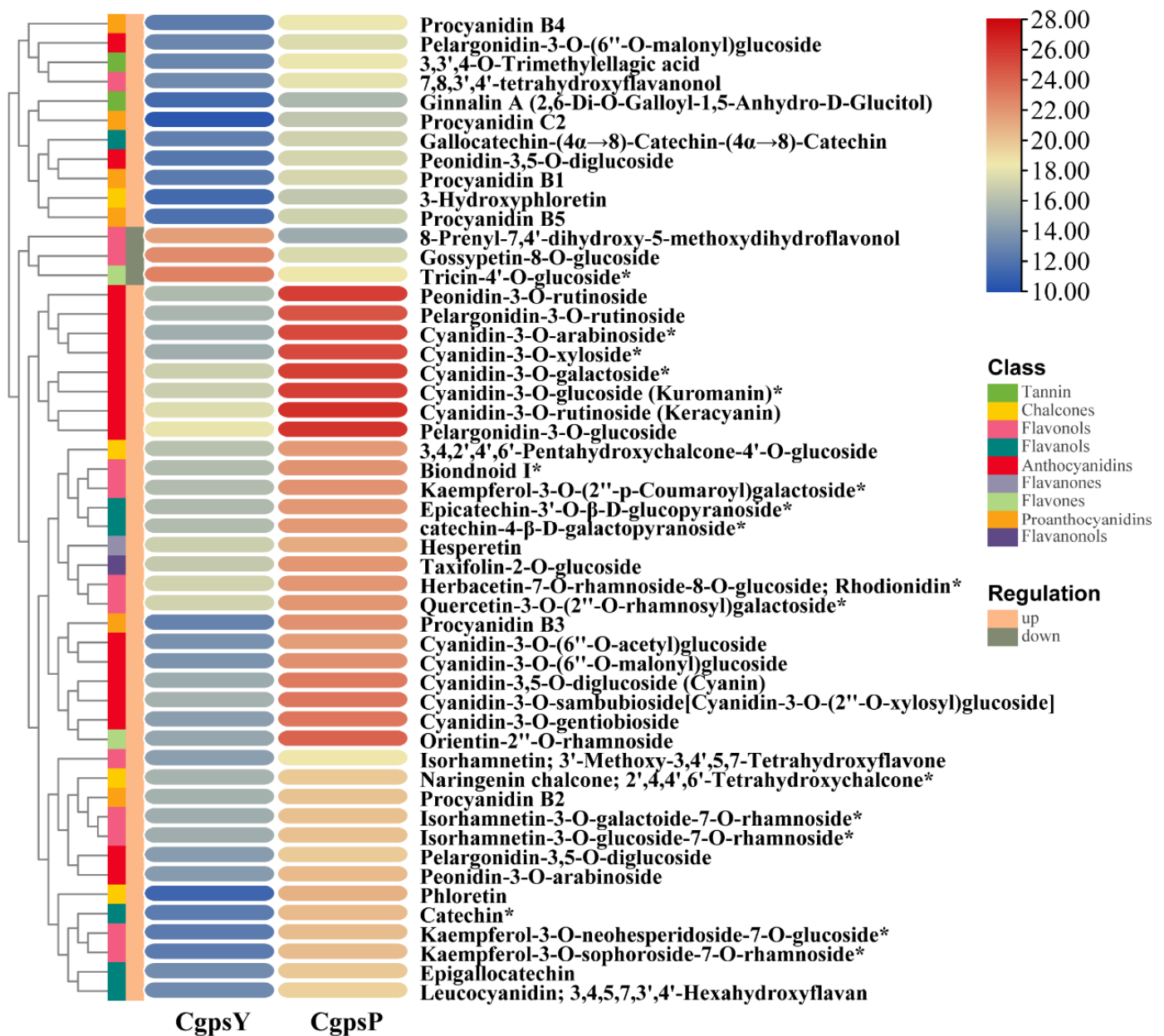


Figure 2. Heatmap of differentially accumulated flavonoid metabolites (DAFs) in CgpsP vs. CgpsY. The figure only shows the differential flavonoid compounds with $|\text{Log}_2\text{FC}| > 4$. The leftmost color bars represent the different flavonoid classes. Each class was assigned a specific color for easy identification (legend right). The up-accumulated and down-accumulated flavonoid compounds are respectively represented in pink and gray bars in the second column from the left. The asterisk denotes the detection of the compound's isomer.

The metabolic compounds implicated in flavonoid biosynthesis (KEGG number: ko00941), anthocyanin biosynthesis (ko00942), and flavone and flavonol biosynthesis (ko00944) were filtered. The most dramatically enriched differentially accumulated metabolite pathways in CgpsP vs. CgpsY were flavonoid biosynthesis (21 compounds out of 28) and flavone, flavonol biosynthesis (14 compounds out of 22), and anthocyanin biosynthesis (11 out of 11).

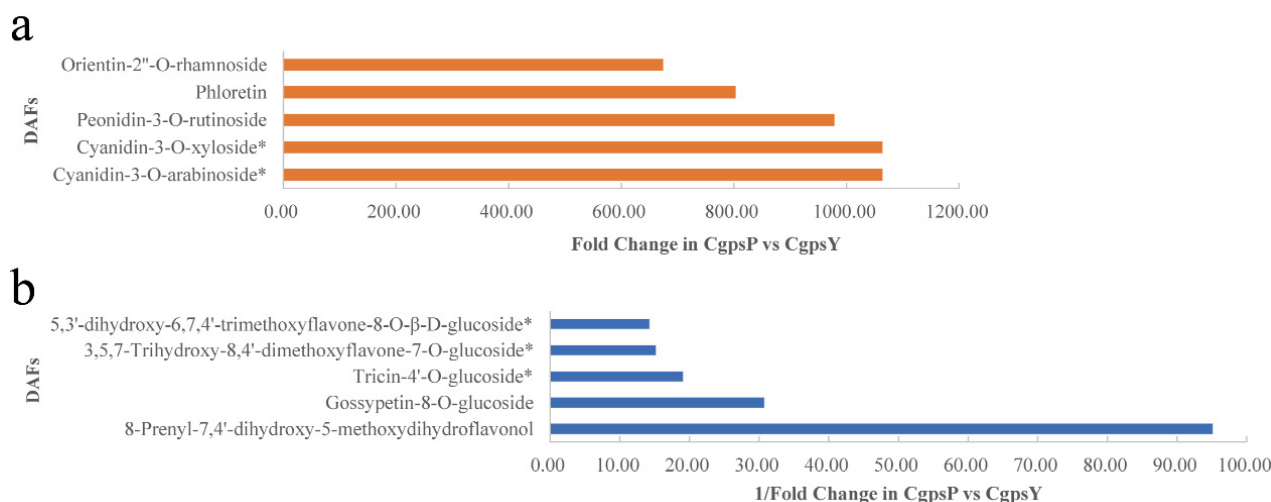


Figure 3. The top 5 upregulated (a) and downregulated (b) DAFs in CggsP vs. CggsY based on the fold change value. The asterisk denotes the detection of the compound's isomer.

3.2. Transcriptome Overview

The transcriptome for the petaloid staminodes of the *C. glauca* wild type (CggsY) and 'Erebus' cultivar (CggsP) was sequenced to identify genes related to pigmentation. In total, 46.12 G clean bases were acquired with an average Q30 of 93%. Six RNA-seq libraries (three for CggsY and three for CggsP) generated 316,126,394 raw reads of 2×150 bp. By eliminating adapters and low-quality reads, 307,540,890 clean reads were acquired for assembly, generating 69,362 unigenes. These unigenes were 1850 bp on average, with an N50 of 2607 bp. Additionally, 24,940 unigenes with a sequence length of at least 2000 bp were identified. These assembled unigenes were annotated using the KEGG, Nr, Swiss-Prot, TrEMBL, KOG, GO, and Pfam, revealing 53,001 unigenes in at least one database. Specifically, 31,995 genes were annotated in KEGG, 52,270 genes were annotated in Nr, 39,081 genes were annotated in Swiss-prot, 52,143 genes were annotated in TrEMBL, 31,483 genes were annotated in the KOG, 44,762 genes were annotated in GO, and 37,922 genes were annotated the in Pfam database. Based on species similarity analysis, the top four similar species, *Musa acuminata* (31.44%, 16,436 unigenes), *Musa troglodytarum* (17.91%, 9359), *Musa balbisiana* (11.69%, 6108), and *Zingiber officinale* (10.61%, 5547), from the same order (Zingiberales) were observed as *C. glauca*.

3.3. Differentially Expressed Genes (DEGs) and Transcription Factors Related to Flavonoid Biosynthesis in Petaloid Staminodes of the Wild Type and Cultivar of *C. glauca*

The transcriptomic analyses of CggsP vs. CggsY provided an overview of alterations in gene expression. In total, 12,057 DEGs, including 6121 upregulated and 5936 downregulated DEGs, were identified with the criterion of two-fold change at $p < 0.05$ (Figure 4a), and the details are available in Supplementary Table S4. These DEGs were enriched in 139 KEGG pathways, including phenylpropanoid biosynthesis (ko00940), flavonoid biosynthesis (ko00941), anthocyanin biosynthesis (ko00942), and flavone and flavonol biosynthesis (ko00944), all of which are associated with flavonoids (Supplementary Table S5). GO enrichment showed that upregulated unigenes outnumbered downregulated unigenes in most of the GO terms (Figure 4b). In particular, 105, 101, 97, 79, and 35 DEGs were respectively enriched in the phenylpropanoid metabolic process, pigment biosynthetic process, secondary metabolite biosynthetic process, phenylpropanoid biosynthetic process, and anthocyanin-containing compound biosynthetic process pathways (Supplementary Figure S2).

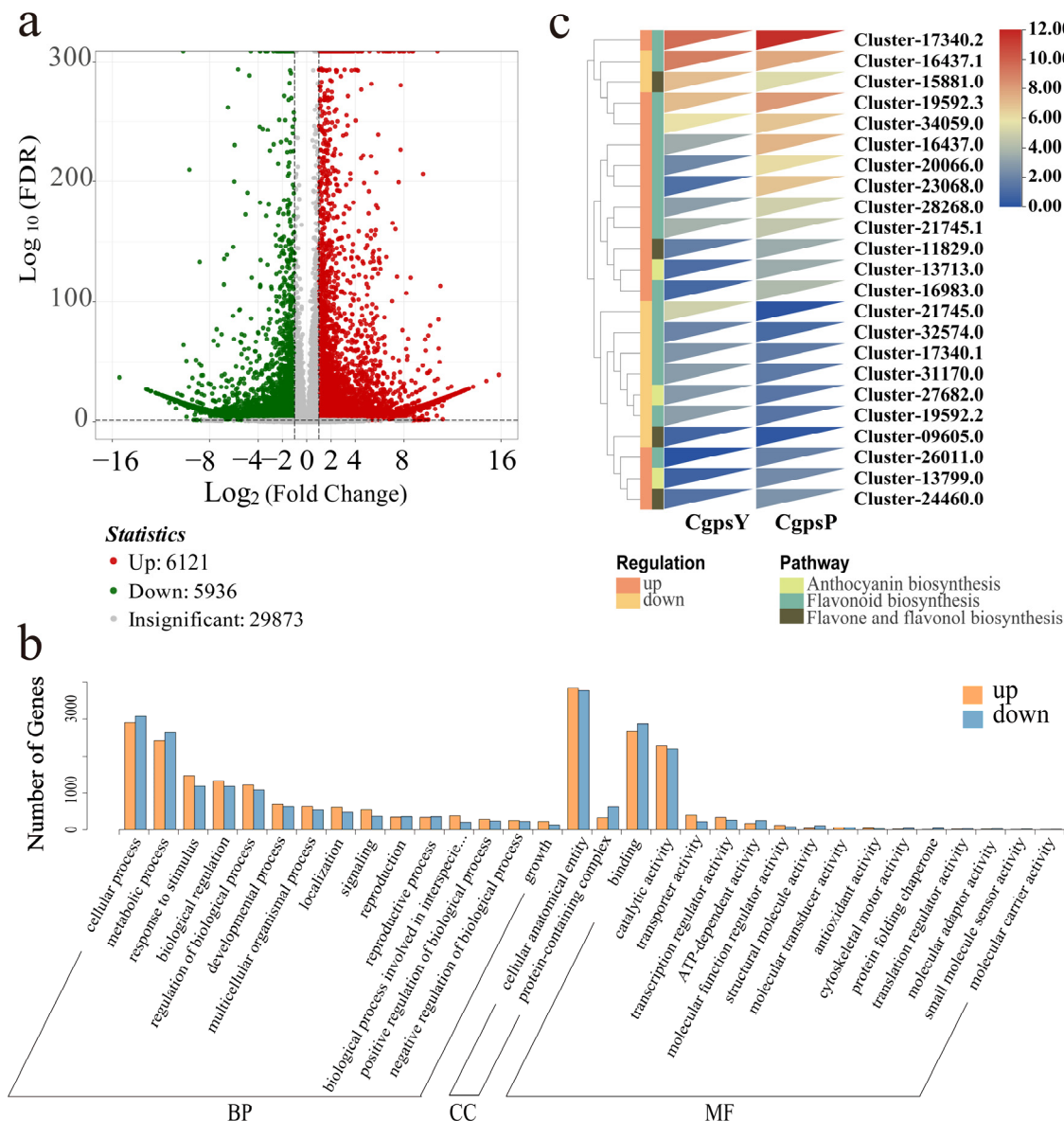


Figure 4. DEGs between the wild type and ‘Erebus’ cultivar of *C. glauca*. (a) The volcano plot illustrating DEGs between CgpsP and CgpsY; (b) GO enrichment of DEGs; (c) expression pattern of DEGs co-enriched in both transcriptome and metabolome KEGG pathways. The genes were clustered by FPKM value with the color scale representing the log₂-transformed FPKM value. The leftmost pink and orange bars indicate upregulated and downregulated DEGs, respectively. The second column from the left shows the different pathways. Each pathway was assigned a specific color for easy identification (legend right).

For better visualization of the connections between genes and metabolites in specific pathways, the differential genes and metabolites of the same comparative group were concurrently plotted on the KEGG pathway map. In CgpsP vs. CgpsY, biosynthesis of secondary metabolites (ko01110, 22 metabolites, 776 genes), metabolic pathways (ko01100, 13 metabolites, 1467 genes), anthocyanin biosynthesis (ko00942, 11 metabolites, 3 genes), flavonoid biosynthesis (ko00941, 21 metabolites, 17 genes), and flavone and flavonol biosynthesis (ko00944, 14 metabolites, 4 genes) pathways were co-enriched in the flavonoid metabolome and transcriptome KEGG pathways. Figure 4c depicts the expression pattern of DEGs involved in flavonoid biosynthesis enriched by both transcriptome and metabolome pathways.

Flavonoid biosynthesis is primarily controlled by external factors and transcription factors (TFs), mainly including MYB and bHLH TFs [34,35]. A total of 3625 TFs were identified, with 783 showing differential expression in CgpsP vs. CgpsY, including bHLH, WRKY, MYB, NAC, MADS-MIKC, MADS-M-type, and AP2/ERF-ERF. Twenty-six TFs were annotated as being in the MYB family, including MYB5, MYB17, MYB23, MYB44 and MYB60. Forty-eight genes encode bHLH TFs. The expression pattern of differentially expressed TFs with the $|\log_2FC| \geq 4.0$ is illustrated in Figure 5, and the details can be found in Supplementary Table S6.

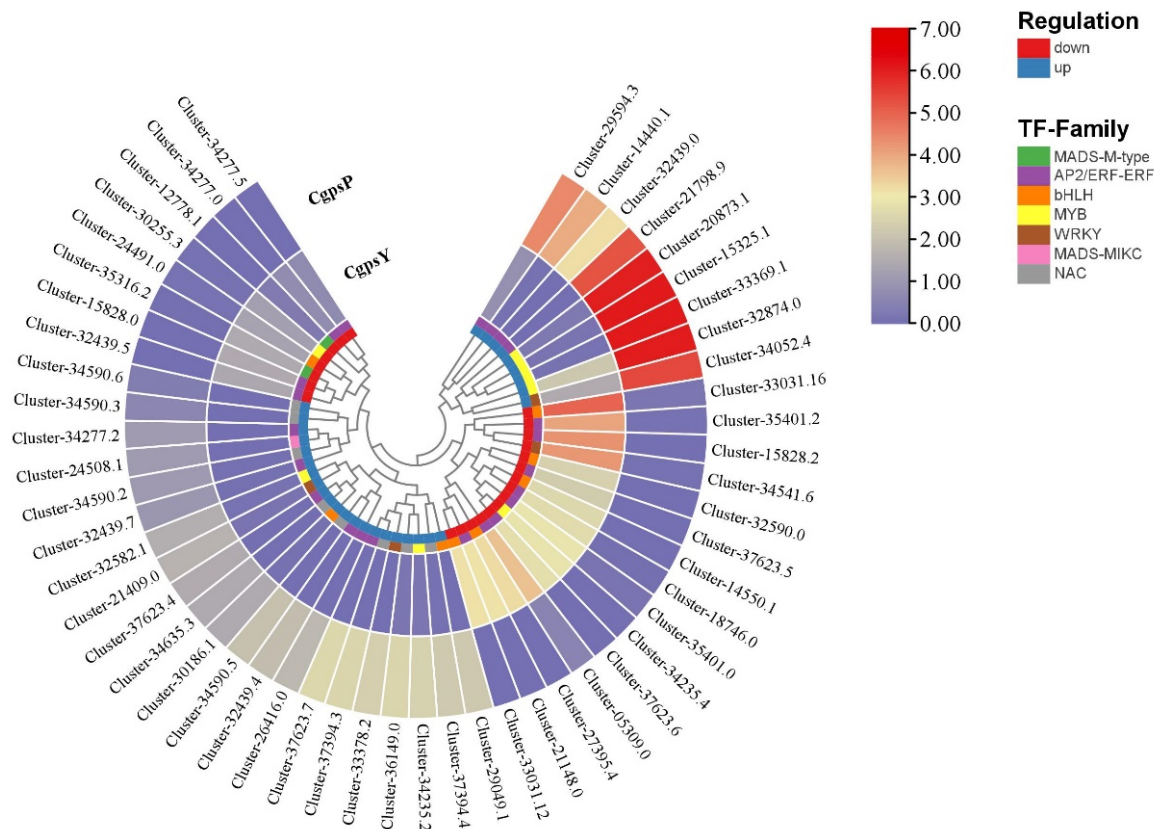


Figure 5. Heatmap illustrating the expression profile of differentially expressed TFs related to the biosynthesis of flavonoid metabolites. TFs with $|\log_2FC| \geq 4.0$ are presented in a color scale reflecting the log-transformed FPKM value, with the color in the innermost circle indicating different TF families and each color in the legend on the right denoting their family identity. Upregulated and downregulated TFs are depicted by blue and red bars, respectively.

Through the analysis of unigenes associated with flavonoids, with a specific emphasis on the anthocyanin biosynthesis pathway, structural genes involved in flavonoid biosynthesis were identified, including *PAL* (1 transcript), *4CL* (2), *C4H* (1), *CHS* (1), *CHI* (3), *F3H* (1), *F3'H* (1), *DFR* (1), *ANS* (1), *UFGT* (10), *FLS* (3), and *AOMT* (1). Figure 6 illustrates the putative genes associated with the flavonoid biosynthesis, along with their expression pattern; the details are shown in Supplementary Table S7. The expression level of *CHS* (Cluster-17340.2), *F3H* (Cluster-16437.0), *DFR* (Cluster-20066.0), *UFGT* (Cluster-36254.1, Cluster-36254.7, Cluster-13799.0, and Cluster-13713.0), and *FLS* (Cluster-26011.0) was significantly upregulated in CgpsP. In contrast, the expression level of *C4H* (Cluster-32574.0), *CHS* (Cluster-17340.1), and *UFGT* (Cluster-36254.0, Cluster-36254.2 and Cluster-27682.0) was significantly downregulated in CgpsP. The levels of these critical genes in the flavonoid biosynthesis pathway dictate the ultimate composition and content of anthocyanins and flavonoids.

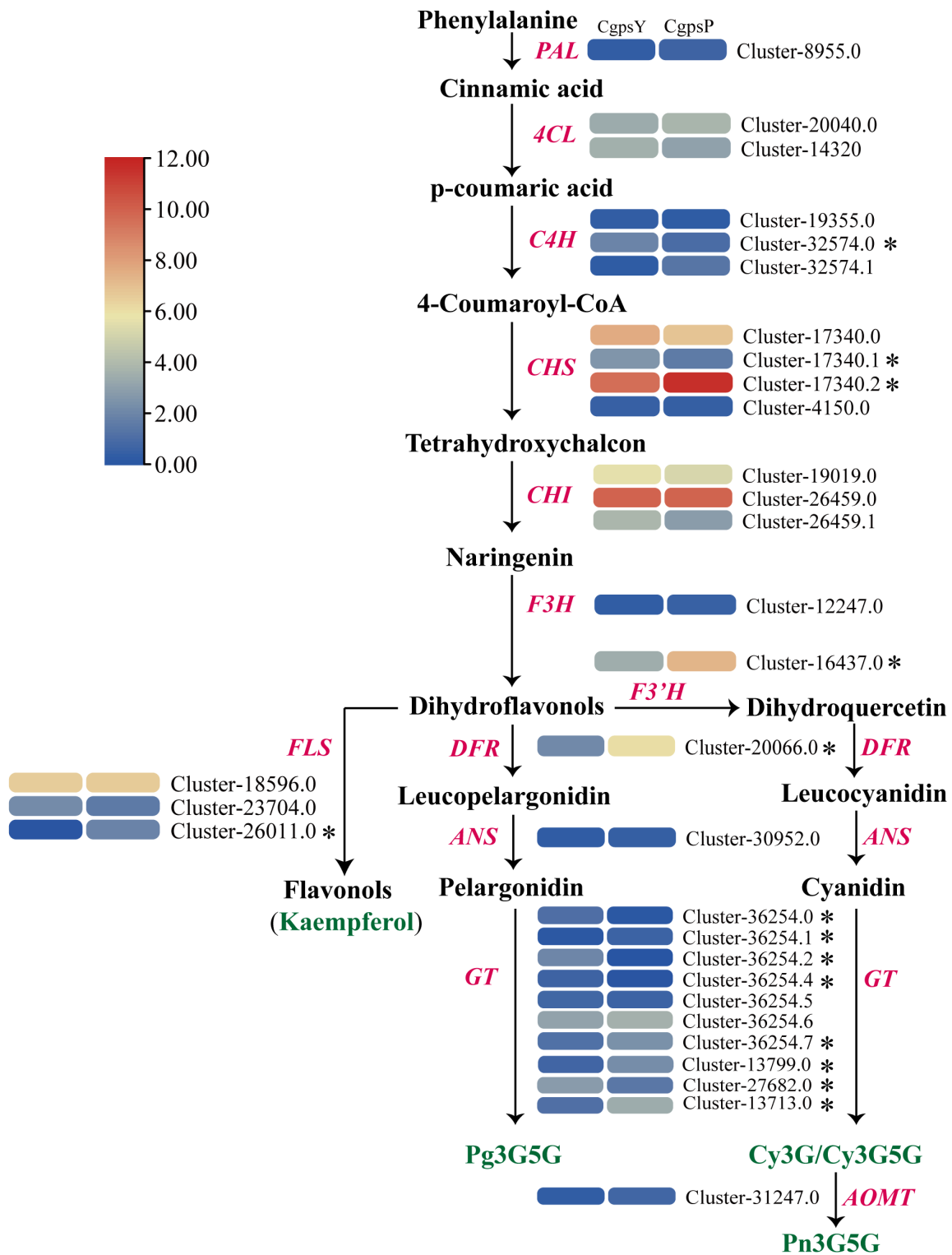


Figure 6. Expression pattern of predicted unigenes implicated in flavonoid biosynthesis in the wild type and ‘Erebus’ cultivar of *C. glauca*. The final flavonoid or anthocyanin metabolites are marked in green. The putative genes are marked in red. The heatmap depicts the expression pattern of each gene corresponding to each step of the pathway in a color scale reflecting the log₂-transformed FPKM values, where red stands for enhanced expression and blue indicates reduced expression in CgpsP vs. CgpsY. The asterisks indicate the DEGs.

3.4. Correlation between DEGs and Anthocyanins

The anthocyanin 3-O-glucosyltransferase (UGT) is pivotal in the final step of anthocyanin synthesis, converting unstable anthocyanins into stable anthocyanins [24,36]. In CgpsP vs. CgpsY, a significant association was observed between the levels of three putative UFGTs (Cluster-13713.0, Cluster-13799.0, and Cluster-27682.0) and 11 anthocyanins (Figure 7, Supplementary Table S8). The expression levels of Cluster-13713.0 and Cluster-13799.0, which were upregulated in CgpsP vs. CgpsY, showed marked positive correlations with the levels of five cyanidins (cyanidin-3,5-O-diglucoside, cyanidin-3-O-(6''-O-malonyl)glucoside, cyanidin-3-O-glucoside, cyanidin-3-O-rutinoside, and cyanidin-3-O-sambubioside), four pelargonidins (pelargonidin-3,5-O-diglucoside, pelargonidin-3-O-(6''-O-malonyl)glucoside, pelargonidin-3-O-glucoside, and pelargonidin-3-O-rutinoside), and one peonidin (peonidin-3-O-glucoside). However, the levels of Cluster-13713.0 and Cluster-13799.0 demonstrated a notable negative correlation with the level of malvidin-3-O-glucoside. Conversely, the level of Cluster-27682.0, which was downregulated in CgpsP vs. CgpsY, exhibited a notable negative correlation with the levels of 10 anthocyanins except for malvidin-3-O-glucoside.

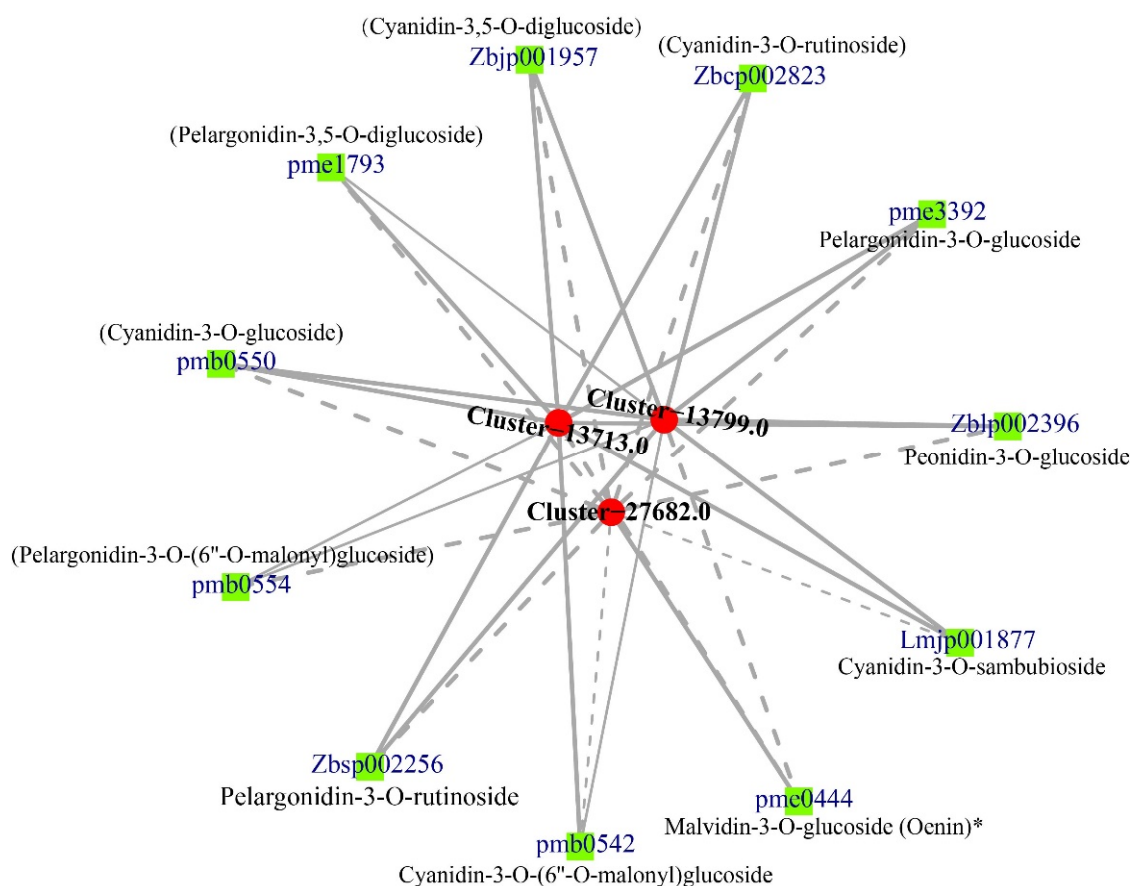


Figure 7. Network diagram of the correlation between 3GT-like genes and anthocyanins. Solid lines indicate positive correlations, while dashed lines represent negative correlations with their thickness reflecting the degree of correlation. The red circles represent the DEGs. The green blocks represent the different types of anthocyanins. The asterisk indicates that the isomer of the compound was detected.

3.5. Real-Time Quantitative PCR Validation

To validate DEGs in the wild type and cultivar of *C. glauca*, we selected nine DEGs related to flavonoid biosynthetic pathways and confirmed their expression using qRT-PCR. Overall, their expression pattern was consistent with the FPKM values obtained

through transcriptome analysis (Supplementary Figure S3), indicating that the measured transcriptome was reliable and effective.

4. Discussion

Flavonoids, including anthocyanins, flavonols, flavones, and proanthocyanidins, are essential for the pigmentation processes of different plants and contribute to the diverse array of colors visible in flowers and fruits. Among them, anthocyanins, produced via the flavonoid biosynthesis pathway, contribute to the vibrant red, purple, and blue hues in plants. Plants produce six major types of anthocyanins, namely cyanidin, delphinidin, peonidin, malvidin, pelargonin, and petunidin, which can impart colors ranging from pink to blue violet [8,9]. *C. glauca*, a horticultural plant with petaloid staminodes as the main ornamental organ, has been widely cultivated in aquatic habitats due to its vibrant flowers and long florescence. In this study, we discovered that the pigment composition in the petaloid staminodes of *C. glauca* mainly comprise 412 flavonoids and 20 anthocyanins. Four types of anthocyanins and their derivatives, mainly including cyanidin, pelargonin, peonidin, and malvidin, were detected in this study. Differential metabolite analysis uncovered a significantly increased abundance of flavonoid compounds in the petaloid staminodes of the 'Erebus' cultivar compared to the wild type. Specifically, the concentration of anthocyanins in 'Erebus' is markedly higher, with greater levels of cyanidin, pelargonidin, peonidin, and their derivatives, whereas the wild type exhibits higher levels of malvidins. Notably, the 'Erebus' cultivar produces over 100 times higher concentrated cyanidins and peonidins than the wild type, whereas the wild type produces over 10 times higher malvidins than the 'Erebus' cultivar. The difference in pigment content accounts for the variation in flower color between the wild type and 'Erebus' cultivar. The overall amount of cyanidins and peonidins dictates the color intensity of the petaloid staminodes of the 'Erebus' cultivar, while the ratio of cyanidins and peonidins governs the hue of the flower color. A recent study in *Alpinia* revealed that the yellow pigments in the labellum were produced by the joint action of flavonoids and carotenoids [14]. The levels of 8-prenyl-7,4'-dihydroxy-5-methoxydihydroflavonol, gossypetin-8-O-glucoside, and triclin-4'-O-glucoside were substantially increased in yellow tissues than in pink tissues, implying their possible participation in the accumulation of yellow pigments. Given the higher total flavonoid content in pink tissue compared to yellow tissue, we propose that flavonoids may not be the main contributor to forming yellow flowers in the wild type of *C. glauca*. In addition to flavonoids, carotenoids could also be involved in the development of yellow pigments, but further investigation is needed.

The modulation of gene expression and enzymatic activities pertaining to flavonoid biosynthesis is essential in determining the types and quantities of flavonoids generated in different plant tissues. One key enzyme in this pathway is *CHS*, which converts 4-coumaroyl-CoA to tetrahydroxy-chalcone. Variations in *CHS* expression levels give rise to the formation of color polymorphism in the flowers of crabapple and arctic mustard [37,38]. We revealed a dramatic enhancement in the *CHS* transcript in the 'Erebus' cultivar compared to the wild type and its correlation with anthocyanin content. *CHI* is another key enzyme in the early stages of flavonoid synthesis. Out of the three *CHI* transcripts identified, only one transcript exhibited a high expression level, with little difference in expression between the pink and yellow tissues. This implies that *CHI* does not have a decisive impact on the flower color variation between the wild type and 'Erebus' cultivar. This finding aligns with a report showing no marked difference in *CHI* expression between the peels of non-red and red apples [39]. *F3'H* emerges as a critical determinant, governing the number of hydroxyls in the B-ring of the anthocyanin aglycon and converting dihydroflavonol to dihydroquercetin [40]. The notably higher expression level of *F3'H* in CgpsP could be responsible for the increased accumulation of cyanidin/peonidin derivatives in the petaloid staminodes of the 'Erebus' cultivar. *DFR*, recognized as a vital enzyme in the late stages of anthocyanin biosynthesis, converts dihydroquercetin into leucoanthocyanins, thus serving as a flavonoid source for the anthocyanin pathway. Variations in *DFR* levels have been

associated with differences in anthocyanin contents and pigmentation patterns in plants including *Dianthus caryophyllus*, crabapples, and *Cymbidium sinense* [41–43]. The elevated expression of *DFR* in CgpsP likely contributes to the higher accumulation of pelargonidin derivatives in the petaloid staminodes of the ‘Erebus’ cultivar. Glycosylation and methylation processes could enhance anthocyanin stability and water solubility, consequently impacting flower coloration in many plants, such as peach, purple celery, blueberries, and blue chrysanthemums [44–47]. Metabolomic analysis revealed peonidins and malvidins as the predominant anthocyanins in CgpsP and CgpsY, respectively, suggesting that methylation occurred in both the ‘Erebus’ cultivar and the wild type.

This study functions as a basis for exploring the biochemical and molecular mechanisms underlying anthocyanin accumulation, offering a theoretical framework for further examination of the gene regulatory network governing anthocyanin biosynthesis in *Canna*.

Supplementary Materials: The supporting information can be downloaded at: <https://www.mdpi.com/article/10.3390/horticulturae10040372/s1>. Figure S1 (The volcano plot illustrating DAFs between CgpsP and CgpsY); Figure S2 (The barplot of GO enrichment of DEGs); Figure S3 (FPKM validation by qRT-PCR); Table S1 (qRT-PCR primers); Table S2 (The flavonoid metabolites detected in the petaloid staminodes of *C. glauca*); Table S3 (The differentially accumulated flavonoids in CgpsP vs. CgpsY); Table S4 (The differentially expressed genes in CgpsP vs. CgpsY); Table S5 (DEGs enriched in the KEGG pathway pertaining to flavonoid biosynthesis in CgpsP vs. CgpsY); Table S6 (Differentially expressed TFs related to the biosynthesis of flavonoid metabolites); Table S7 (Expression pattern of predicted unigenes implicated in flavonoid biosynthesis in the wild type and ‘Erebus’ cultivar of *C. glauca*); Table S8 (The correlation between DEGs and anthocyanins).

Author Contributions: T.Z. conceived the study, executed the experiments, examined the data, and authored the paper. Z.W. analyzed and visualized the data. H.L. contributed to the data analysis. L.D. helped with sample collection and contributed to language refinement. All authors have read and agreed to the published version of the manuscript.

Funding: This research was sponsored by Guangdong Ordinary University Characteristic Innovation Project (grant number 2022KTSCX285); Guangdong Basic and Applied Basic Research Foundation (grant number 2021A1515110529); and Guangdong Ordinary University Special Projects in Key Fields (grant number 2023ZDZX4106).

Data Availability Statement: The RNA-seq data have been archived in the National Center for Biotechnology Information Short Read Archive (NCBI-SRA) database (<https://www.ncbi.nlm.nih.gov/Traces/sra> (accessed on 31 October 2023)), and assigned the accession number PRJNA1034286.

Acknowledgments: We appreciate Wensu He for his assistance with the sample collection.

Conflicts of Interest: The authors declare no conflicts of interest.

References

1. Dahlgren, R.M.T.; Rasmussen, F. Monocotyledon evolution: Characters and phylogenetic estimation. In *Evolutionary Biology*; Springer: Boston, MA, USA, 1983; Volume 16, pp. 255–395.
2. Kirchoff, B.K. Floral ontogeny and evolution in the ginger group of the Zingiberales. In *Aspects of Floral Development*; Leins, P., Tucker, S.C., Eds.; Cramer: Berlin, Germany, 1988; pp. 45–56.
3. Kress, W.J. The Phylogeny and classification of the Zingiberales. *Ann. Mo. Bot. Gard.* **1990**, *77*, 698–721. [[CrossRef](#)]
4. Kirchoff, B.K. Floral organogenesis in five genera of the Marantaceae and in *Canna* (Cannaceae). *Am. J. Bot.* **1983**, *70*, 508–523. [[CrossRef](#)]
5. Miao, M.; Liu, H.; Kuang, Y.; Zou, P.; Liao, J. Floral vasculature and ontogeny in *Canna indica*. *Nord. J. Bot.* **2014**, *32*, 485–492. [[CrossRef](#)]
6. Tanaka, Y.; Brugliera, F.; Chandler, S. Recent progress of flower colour modification by biotechnology. *Int. J. Mol. Sci.* **2009**, *10*, 5350–5369. [[CrossRef](#)]
7. Petroni, K.; Tonelli, C. Recent advances on the regulation of anthocyanin synthesis in reproductive organs. *Plant Sci.* **2011**, *181*, 219–229. [[CrossRef](#)]
8. Martin, C.; Prescott, A.; Mackay, S.; Bartlett, J.; Vrijlandt, E. Control of anthocyanin biosynthesis in flowers of *Antirrhinum majus*. *Plant J.* **1991**, *1*, 37–49. [[CrossRef](#)]
9. Kazuma, K.; Noda, N.; Suzuki, M. Flavonoid composition related to petal color in different lines of *Clitoria ternatea*. *Phytochemistry* **2003**, *64*, 1133–1139. [[CrossRef](#)]

10. Peng, J.; Dong, X.; Xue, C.; Liu, Z.; Cao, F. Exploring the molecular mechanism of blue flower color formation in *Hydrangea macrophylla* cv. "Forever Summer". *Front. Plant Sci.* **2021**, *12*, 585665. [[CrossRef](#)]
11. Grotewold, E. The genetics and biochemistry of floral pigments. *Annu. Rev. Plant Biol.* **2006**, *57*, 761–780. [[CrossRef](#)]
12. Zhang, Y.; Butelli, E.; Martin, C. Engineering anthocyanin biosynthesis in plants. *Curr. Opin. Plant Biol.* **2014**, *19*, 81–90. [[CrossRef](#)]
13. Zhao, D.; Tao, J. Recent advances on the development and regulation of flower color in ornamental plants. *Front. Plant Sci.* **2015**, *6*, 261. [[CrossRef](#)]
14. Zhang, H.; Yuan, X.; Wang, R.; Wang, L.; Gao, J.; Wang, H.; Li, Y.; Fu, Z. Comprehensive transcriptome and metabolome characterization of peony 'Coral Sunset' petals provides insights into the mechanism of pigment degradation. *Horticulturae* **2023**, *9*, 1295. [[CrossRef](#)]
15. Zhao, T.; Yu, Q.; Lin, C.; Liu, H.; Dong, L.; Feng, X.; Liao, J. Analyzing morphology, metabolomics, and transcriptomics offers invaluable insights into the mechanisms of pigment accumulation in the diverse-colored labellum tissues of *Alpinia*. *Plants* **2023**, *12*, 3766. [[CrossRef](#)]
16. Wang, R.; Ren, C.; Dong, S.; Chen, C.; Xian, B.; Wu, Q.; Wang, J.; Pei, J.; Chen, J. Integrated metabolomics and transcriptome analysis of flavonoid biosynthesis in safflower (*Carthamus tinctorius* L.) with different colors. *Front. Plant Sci.* **2021**, *12*, 712038. [[CrossRef](#)]
17. Fu, M.; Yang, X.; Zheng, J.; Wang, L.; Yang, X.; Tu, Y.; Ye, J.; Zhang, W.; Liao, Y.; Cheng, S.; et al. Unraveling the regulatory mechanism of color diversity in *Camellia japonica* petals by integrative transcriptome and metabolome analysis. *Front. Plant Sci.* **2021**, *12*, 685136. [[CrossRef](#)]
18. Nishihara, M.; Nakatsuka, T. Genetic engineering of novel flower colors in floricultural plants: Recent advances via transgenic approaches. *Methods Mol. Biol.* **2010**, *589*, 325–347.
19. Nishihara, M.; Nakatsuka, T. Genetic engineering of flavonoid pigments to modify flower color in floricultural plants. *Biotechnol. Lett.* **2011**, *33*, 433–441. [[CrossRef](#)]
20. Jin, X.; Huang, H.; Wang, L.; Sun, Y.; Dai, S. Transcriptomics and metabolite analysis reveals the molecular mechanism of anthocyanin biosynthesis branch pathway in different *Senecio cruentus* cultivars. *Front. Plant Sci.* **2016**, *7*, 1307. [[CrossRef](#)]
21. Xu, L.; Yang, P.; Feng, Y.; Xu, H.; Cao, Y.; Tang, Y.; Yuan, S.; Liu, X.; Ming, J. Spatio temporal transcriptome analysis provides insights into bicolor tepal development in *Lilium* "Tiny Padhye". *Front. Plant Sci.* **2017**, *8*, 398. [[CrossRef](#)]
22. Li, L.; Ye, J.; Li, H.; Shi, Q. Characterization of metabolites and transcripts involved in flower pigmentation in *Primula vulgaris*. *Front. Plant Sci.* **2020**, *11*, 572517. [[CrossRef](#)]
23. Ma, Y.; Duan, H.; Zhang, F.; Li, Y.; Yang, H.-S.; Tian, F.-P.; Zhou, X.-H.; Wang, C.-M.; Ma, R. Transcriptomic analysis of *Lycium ruthenicum* Murr. during fruit ripening provides insight into structural and regulatory genes in the anthocyanin biosynthetic pathway. *PLoS ONE* **2018**, *13*, e0208627. [[CrossRef](#)]
24. Hichri, I.; Barrieu, F.; Bogs, J.; Kappel, C.; Delrot, S.; Lauvergeat, V. Recent advances in the transcriptional regulation of the flavonoid biosynthetic pathway. *J. Exp. Bot.* **2011**, *62*, 2465–2483. [[CrossRef](#)]
25. Yin, X.; Lin, X.; Liu, Y.; Irfan, M.; Chen, L.; Zhang, L. Integrated metabolic profiling and transcriptome analysis of pigment accumulation in diverse petal tissues in the lily cultivar 'Vivian'. *BMC Plant Biol.* **2020**, *20*, 446. [[CrossRef](#)]
26. Luo, X.; Sun, D.; Wang, S.; Luo, S.; Fu, Y.; Niu, L.; Shi, Q.; Zhang, Y. Integrating full-length transcriptomics and metabolomics reveals the regulatory mechanisms underlying yellow pigmentation in tree peony (*Paeonia suffruticosa* Andr.) flowers. *Hort. Res.* **2021**, *1*, 008.
27. Chen, C.; Wu, Y.; Li, J.; Wang, X.; Zeng, Z.; Xu, J.; Liu, Y.; Feng, J.; Chen, H.; He, Y.; et al. TBtools-II: A "one for all, all for one" bioinformatics platform for biological big-data mining. *Mol. Plant* **2023**, *16*, 1733–1742. [[CrossRef](#)]
28. He, J.; Jiao, Y. Next-generation sequencing applied to flower development: RNA-seq. In *Flower Development: Methods and Protocols*; Riechmann, J.L., Wellmer, F., Eds.; Springer: New York, NY, USA, 2014; Volume 1110, pp. 401–411.
29. Grabherr, M.G.; Haas, B.J.; Yassour, M.; Levin, J.Z.; Thompson, D.A.; Amit, I.; Adiconis, X.; Fan, L.; Raychowdhury, R.; Zeng, Q.; et al. Trinity: Reconstructing a full-length transcriptome without a genome from RNA-Seq data. *Nat. Biotechnol.* **2011**, *29*, 644–652. [[CrossRef](#)]
30. Conesa, A.; Götz, S.; García-Gómez, J.M.; Terol, J.; Talón, M.; Robles, M. Blast2GO: A universal tool for annotation, visualization and analysis in functional genomics research. *Bioinformatics* **2005**, *21*, 3674–3676. [[CrossRef](#)]
31. Mortazavi, A.; Williams, B.; McCue, K.; Schaeffer, L.; Wold, B. Mapping and quantifying mammalian transcriptomes by RNA-Seq. *Nat. Methods* **2008**, *5*, 621–628. [[CrossRef](#)]
32. Robinson, M.D.; McCarthy, D.J.; Smyth, G.K. edgeR: A Bioconductor package for differential expression analysis of digital gene expression data. *Bioinformatics* **2009**, *26*, 139–140. [[CrossRef](#)]
33. Livak, K.J.; Schmittgen, T.D. Analysis of relative gene expression data using real-time quantitative PCR and the $2^{-\Delta\Delta Ct}$ method. *Methods* **2001**, *25*, 402–408. [[CrossRef](#)]
34. Jian, W.; Cao, H.H.; Yuan, S.; Liu, Y.D.; Lu, J.; Lu, W.; Li, N.; Wang, J.; Zou, J.; Tang, N.; et al. SIMYB75, an MYB-type transcription factor, promotes anthocyanin accumulation and enhances volatile aroma production in tomato fruits. *Hortic. Res.* **2019**, *6*, 22. [[CrossRef](#)] [[PubMed](#)]
35. Xie, X.B.; Li, S.; Zhang, R.F.; Zhao, J.; Chen, Y.; Zhao, Q.; Yao, Y.; You, C.; Zhang, X.; Hao, Y. The bHLH transcription factor MdbHLH3 promotes anthocyanin accumulation and fruit colouration in response to low temperature in apples. *Plant Cell Environ.* **2012**, *35*, 1884–1897. [[PubMed](#)]

36. Misyura, M.; Colasanti, J.; Rothstein, S.J. Physiological and genetic analysis of *Arabidopsis thaliana* anthocyanin biosynthesis mutants under chronic adverse environmental conditions. *J. Exp. Bot.* **2013**, *64*, 229–240. [[CrossRef](#)] [[PubMed](#)]
37. Tai, D.; Tian, J.; Zhang, J.; Song, T.; Yao, Y. *Malus* crabapple chalcone synthase gene, *McCHS*, regulates red petal color and flavonoid biosynthesis. *PLoS ONE* **2014**, *9*, 110570. [[CrossRef](#)] [[PubMed](#)]
38. Dick, C.; Buenrostro, J.; Butler, T.; Carlson, M.L.; Kliebenstein, D.J.; Whittall, J.B. Arctic mustard flower color polymorphism controlled by petal-specific downregulation at the threshold of the anthocyanin biosynthetic pathway. *PLoS ONE* **2011**, *6*, 18230. [[CrossRef](#)]
39. Takos, A.; Jaffé, F.; Jacob, S.; Bogs, J.; Robinson, S.P.; Walker, A.R. Light induced expression of a *MYB* gene regulates anthocyanin biosynthesis in red apples. *Plant Physiol.* **2006**, *142*, 1216–1232. [[CrossRef](#)] [[PubMed](#)]
40. Sunil, L.; Shetty, N.P. Biosynthesis and regulation of anthocyanin pathway genes. *Appl. Microbiol. Biot.* **2022**, *106*, 1783–1798. [[CrossRef](#)] [[PubMed](#)]
41. Stich, K.; Eidenberger, T.; Wurst, F.; Forkmann, G. Enzymatic conversion of dihydroflavonols to flavan-3, 4-diols using flower extracts of *Dianthus caryophyllus* L. (carnation). *Planta* **1992**, *187*, 103–108. [[CrossRef](#)] [[PubMed](#)]
42. Tian, J.; Han, Z.; Zhang, J.; Hu, Y.; Song, T.; Yao, Y. The balance of expression of dihydroflavonol 4-reductase and flavonol synthase regulates flavonoid biosynthesis and red foliage coloration in crabapples. *Sci. Rep.* **2015**, *5*, 12228. [[CrossRef](#)]
43. Gao, J.; Ren, R.; Wei, Y.; Jin, J.; Ahmad, S.; Lu, C.; Wu, J.; Zheng, C.; Yang, F.; Zhu, G. Comparative metabolomic analysis reveals distinct flavonoid biosynthesis regulation for leaf color development of *Cymbidium sinense* ‘Red Sun’. *Int. J. Mol. Sci.* **2020**, *21*, 1869–1886. [[CrossRef](#)]
44. Noda, N.; Yoshioka, S.; Kishimoto, S.; Nakayama, M.; Douzono, M.; Tanaka, Y.; Aida, R. Generation of blue chrysanthemums by anthocyanin B-ring hydroxylation and glucosylation and its coloration mechanism. *Sci. Adv.* **2017**, *3*, e1602785. [[CrossRef](#)] [[PubMed](#)]
45. Cheng, J.; Wei, G.; Zhou, H.; Gu, C.; Vimolmangkang, S.; Liao, L.; Han, Y. Unraveling the mechanism underlying the glycosylation and methylation of anthocyanins in peach. *Plant Physiol.* **2014**, *166*, 1044–1058. [[CrossRef](#)] [[PubMed](#)]
46. Feng, K.; Xu, Z.; Liu, J.; Li, J.; Wang, F.; Xiong, A. Isolation, purification, and characterization of *AgUCGalT1*, a galactosyltransferase involved in anthocyanin galactosylation in purple celery (*Apium graveolens* L.). *Planta* **2018**, *247*, 1363–1375. [[CrossRef](#)]
47. Xie, L.; Lu, Y.; Zhou, Y.; Hao, X.; Chen, W. Functional analysis of a methyltransferase involved in anthocyanin biosynthesis from blueberries (*Vaccinium corymbosum*). *J. Agric. Food Chem.* **2022**, *70*, 16253–16262. [[CrossRef](#)] [[PubMed](#)]

Disclaimer/Publisher’s Note: The statements, opinions and data contained in all publications are solely those of the individual author(s) and contributor(s) and not of MDPI and/or the editor(s). MDPI and/or the editor(s) disclaim responsibility for any injury to people or property resulting from any ideas, methods, instructions or products referred to in the content.